

Article

## Silicon Heterojunction Solar Cells Using $\text{AlO}_x$ and Plasma-Immersion Ion Implantation

Yu-Hsien Lin <sup>1</sup>, Yung-Chun Wu <sup>2,\*</sup>, Hsin-Chiang You <sup>3</sup>, Chun-Hao Chen <sup>2</sup>, Ping-Hua Chen <sup>1</sup>, Yi-He Tsai <sup>1</sup>, Yi-Yun Yang <sup>1</sup> and K. S. Chang-Liao <sup>2</sup>

<sup>1</sup> Department of Electronic Engineering, National United University, No. 1, Lienda, Miaoli 36003, Taiwan; E-Mails: yhlin@nuu.edu.tw (Y.-H.L.); c510135@yahoo.com.tw (P.-H.C.); tsaiyihe@gmail.com (Y.-H.T.); u0022034@nuu.edu.tw (Y.-Y.Y.)

<sup>2</sup> Department of Engineering and System Science, National Tsing Hua University, No. 101, Section 2, Kuang-Fu Road, Hsinchu, 30013, Taiwan; E-Mails: n124307124@gmail.com (C.-H.C.); lkschang@ess.nthu.edu.tw (K.S.C.-L.)

<sup>3</sup> Department of Electronic Engineering, National Chin-Yi University of Technology, No. 57, Sec. 2, Zhongshan Rd., Taiping Dist., Taichung 41170, Taiwan; E-Mail: hcyou@ncut.edu.tw

\* Author to whom correspondence should be addressed; E-Mail: ycwu@ess.nthu.edu.tw; Tel.: +886-3-571-5131 (ext. 34287); Fax: +886-3-572-0724.

Received: 13 March 2014; in revised form: 20 May 2014 / Accepted: 5 June 2014 /

Published: 13 June 2014

---

**Abstract:** Aluminum oxide ( $\text{AlO}_x$ ) and plasma immersion ion implantation (PIII) were studied in relation to passivated silicon heterojunction solar cells. When aluminum oxide ( $\text{AlO}_x$ ) was deposited on the surface of a wafer; the electric field near the surface of wafer was enhanced; and the mobility of the carrier was improved; thus reducing carrier traps associated with dangling bonds. Using PIII enabled implanting nitrogen into the device to reduce dangling bonds and achieve the desired passivation effect. Depositing  $\text{AlO}_x$  on the surface of a solar cell increased the short-circuit current density ( $J_{sc}$ ); open-circuit voltage ( $V_{oc}$ ); and conversion efficiency from 27.84 mA/cm<sup>2</sup>; 0.52 V; and 8.97% to 29.34 mA/cm<sup>2</sup>; 0.54 V; and 9.68%; respectively. After controlling the depth and concentration of nitrogen by modulating the PIII energy; the ideal PIII condition was determined to be 2 keV and 10 min. As a result; a 15.42% conversion efficiency was thus achieved; and the  $J_{sc}$ ;  $V_{oc}$ ; and fill factor were 37.78 mA/cm<sup>2</sup>; 0.55 V; and 0.742; respectively.

**Keywords:** plasma-immersion ion implantation; silicon heterojunction; solar cell

---

## 1. Introduction

As conventional energy sources such as coal, oil, and natural gas are exhausted, solar energy is becoming increasingly crucial [1–13]. The combustion of fossil fuels produces carbon dioxide, which causes the greenhouse effect. Protecting the environment for the next generation is vital; alternative energy sources must be investigated, and renewable energy technologies must be developed to counteract the greenhouse effect. Green energy is a major area of academic and industrial research, and steep increases in petroleum prices have renewed the focus on alternative sources of energy.

In many applications, amorphous silicon/crystalline silicon (a-Si/c-Si) heterojunction solar cells offer several advantages. First, they yield increased open-circuit voltage ( $V_{oc}$ ) because of their a-Si structure [14]; the band-gap of a-Si is wider than that of c-Si; thus, the  $V_{oc}$  of a-Si/c-Si heterojunction solar cells is larger than that of homojunction solar cells. Second, the electric field at the interface of an a-Si/c-Si solar cell is larger than that of a homojunction solar cell [15]. As shown in the energy band diagram, the structure of a-Si/c-Si cell is more beveled than the homojunction structure. Third, a-Si/c-Si heterojunction solar cells are more efficient than homojunction solar cells [16]. Finally, a-Si/c-Si heterojunction solar cells are more effective for generating electric power than a-Si thin film solar cells at high temperatures [17].

In this study, an  $AlO_x$  layer was deposited on the surface of an a-Si/c-Si heterojunction solar cell. It was expected that the field-effect passivation would improve the short-circuit current density ( $J_{sc}$ ) and  $V_{oc}$ . Because a-Si and c-Si interfaces have substantial amounts of defects [13], enhancing the electric fields near a-Si and c-Si interfaces can improve carrier mobility and reduce carrier traps at the interfaces.

Plasma immersion ion implantation (PIII) was used in this study to enhance performance [18–20]. The target received substantial negative pulse voltage, and plasma was formed by the RF power in the cavity. Simultaneously, nitrogen was imported to produce positively charged nitrogen ions, and the plasma ions implanted nitrogen in the device from all sides. This method allowed for lower implantation energy and higher doses, thereby reducing the number of device defects from ion implantation. PIII was used to reduce the number of dangling bonds in the solar cell.

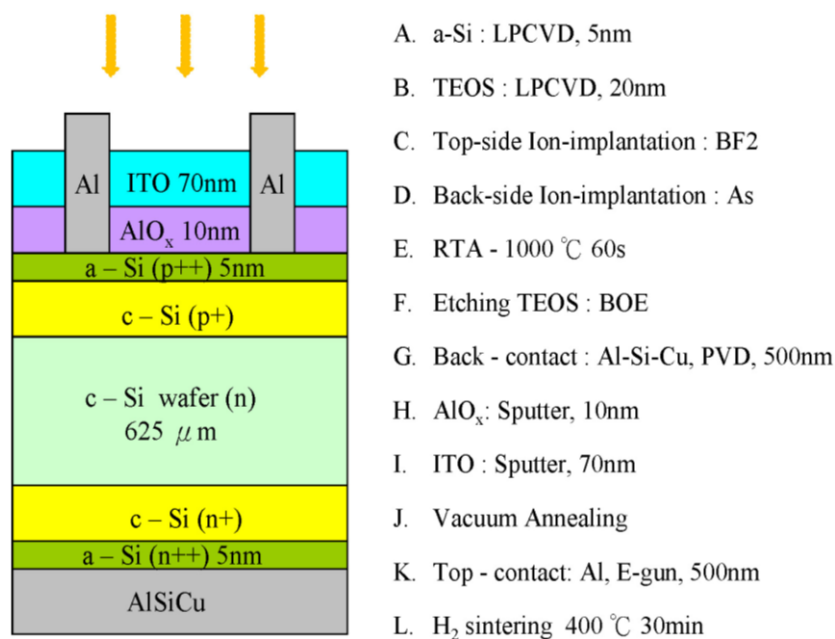
## 2. Experimental Section

Figure 1 shows the structure of the solar cell device. After RCA cleaning, an LPCVD furnace was used to deposit a-Si 50 Å to create a heterojunction solar cell; a solar cell without a-Si was also created as a homojunction solar cell. Second,  $SiO_2$  was deposited as a PIII buffer layer. PIII was then applied to the top and back sides of the wafer (60 tilt, 40 keV, source  $BF_2$ , and 7 tilt, 40 keV, source As). After implantation, rapid thermal annealing (1,000 °C, 60 s) was used to activate the ions, followed by etching the  $SiO_2$  by using BOE. AlSiCu (5,000 Å) was deposited using PVD on the back contact, and  $H_2$  sintering (400 °C, 30 min) was conducted using a furnace.

The basic homojunction (without a-Si) and heterojunction (with a-Si) devices were fabricated as follows. A metal mask was used to define the pattern of the front contact, following the application of 10-nm  $AlO_x$  on the top of the cells using DC sputtering. Subsequently, DC sputtering was used to deposit a 70-nm ITO ARC-layer on the tops of the cells. Front contact electrodes of 5,000 Å (500 nm)

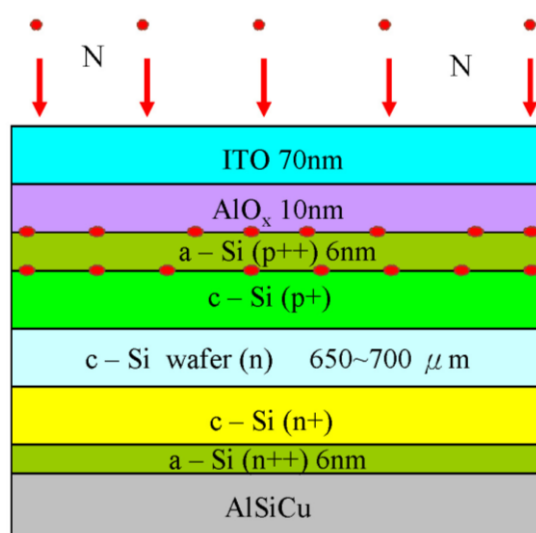
Al were applied using electron beam evaporation. Finally, the cells were cut into  $1 \times 1 \text{ cm}^2$  pieces to measure solar cell efficiency. Three solar cells were fabricated, including a heterojunction solar cell with  $\text{AlO}_x$  passivation, and one without  $\text{AlO}_x$  passivation.

**Figure 1.** Heterojunction solar cell with  $\text{AlO}_x$  passivation.



The use of nitrogen to passivate dangling bonds on a-Si and c-Si solar cell surfaces using PIII was investigated (Figure 2). PIII energy at 2 keV, 4 keV, 6 keV, and 5 min, 10 min, and 15 min of PIII time, were investigated. The short-circuit current ( $I_{sc}$ ),  $V_{oc}$ , fill factor (FF), and conversion efficiency ( $\zeta$ ) of the solar cell devices were subsequently compared.

**Figure 2.** Passivated solar cell by using PIII.



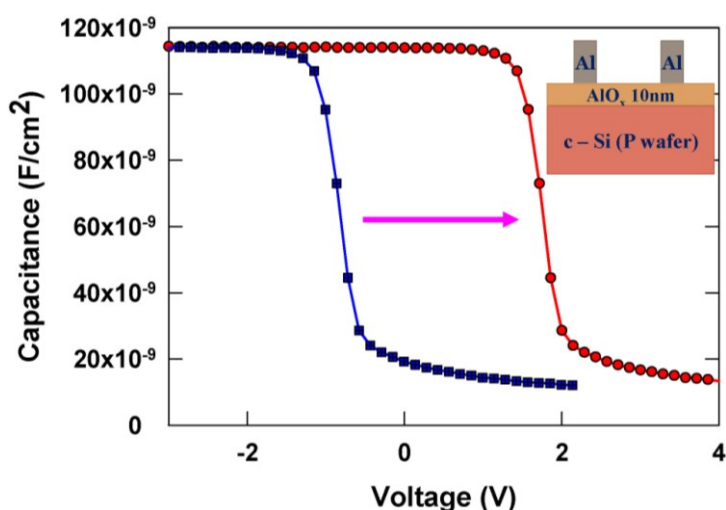
The comparison is shown on Table 1. Depositing  $\text{AlO}_x$  on the surface of a solar cell increased the short-circuit current density ( $J_{sc}$ ), open-circuit voltage ( $V_{oc}$ ), and conversion efficiency from  $27.84 \text{ mA/cm}^2$ , 0.52 V, and 8.97% to  $29.34 \text{ mA/cm}^2$ , 0.54 V, and 9.68%, respectively.

### 3. Results and Discussion

#### 3.1. AlO<sub>x</sub> Measurement and Analysis

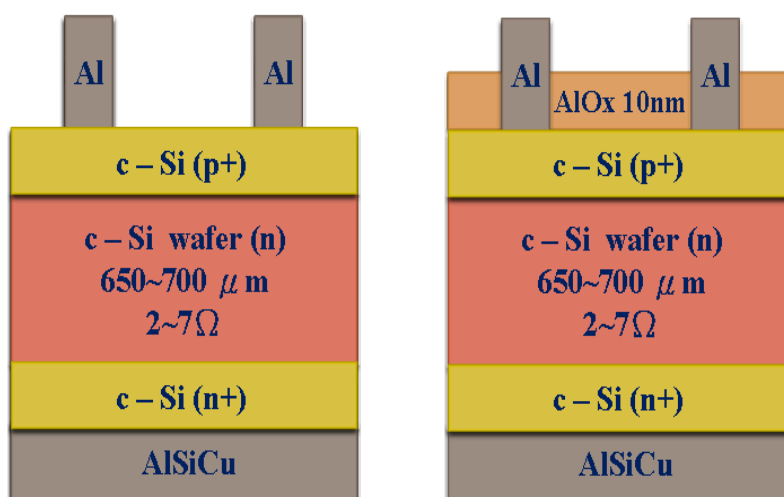
AlO<sub>x</sub> was deposited on the solar cells to passivate the surface by a fixed charge, thereby inducing the field-effect. The number of fixed charges on the AlO<sub>x</sub>/c-Si interface was determined. AlO<sub>x</sub> was used to fabricate the AlO<sub>x</sub>/c-Si capacitance (insert in Figure 3), and the capacitance-voltage (C-V) curve was measured (Figure 3). The area of the capacitance is 50 × 50 μm<sup>2</sup>. From the C-V characteristics in Figure 3, we can find the flat-band voltage was 2.7 V by voltage sweeping. As a result, we can obtain fixed charges on the AlO<sub>x</sub>/c-Si interface in 10<sup>12</sup> cm<sup>-2</sup>. The CV curve shows right shifting, it reveals that the negative charges exist in AlO<sub>x</sub>, and induce an accumulation layer at the p-type silicon interface, resulting in a very effective field-effect passivation [21,22].

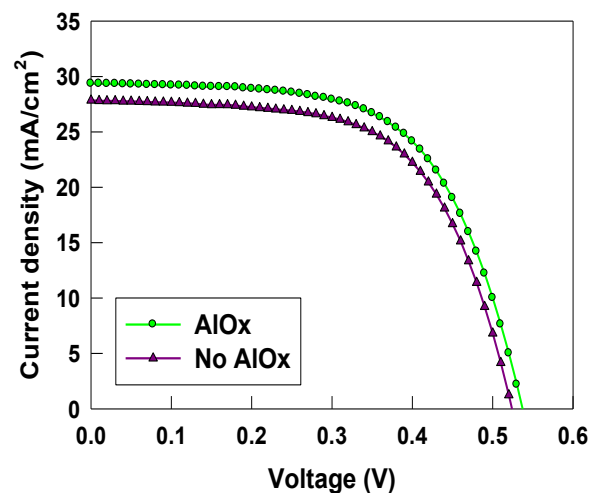
Figure 3. Basic structure of AlO<sub>x</sub>/c-Si capacitance.



As shown in Figure 4, we compared two structures of the homojunction solar cells with and without AlO<sub>x</sub> passivation samples, both without ITO ARC-layers. As shown by the characteristic I-V curve in Figure 5, the  $J_{sc}$ ,  $V_{oc}$ , and  $\eta$  were increased by AlO<sub>x</sub> passivation.

Figure 4. Comparison of without AlO<sub>x</sub> and with AlO<sub>x</sub> structure.



**Figure 5.** The I-V characteristic curve of without AlO<sub>x</sub> and with AlO<sub>x</sub> samples.**Table 1.** The summary table of without AlO<sub>x</sub> and with AlO<sub>x</sub> homojunction solar cells.

Description	w/o AlO <sub>x</sub>	w/i AlO <sub>x</sub>
$J_{sc}$ (mA/cm <sup>2</sup> )	27.84	29.34
$V_{oc}$ (V)	0.52	0.54
FF	0.62	0.611
$\zeta$ (%)	8.97	9.68

### 3.2. PIII Measurement and Analysis

The use of nitrogen to passivate dangling bonds on a-Si and c-Si surfaces by using PIII was investigated. To control the nitrogen depth, three PIII energy conditions of homojunction solar cells with AlO<sub>x</sub> passivation were studied: 2 keV, 4 keV, and 6 keV in 10 min. Based on the I-V curves in Figure 6 and Table 2, the PIII at 2 keV yielded a superior passivation effect. The short-circuit current density ( $J_{sc}$ ), open-circuit voltage ( $V_{oc}$ ), and conversion efficiency were 37.95 mA/cm<sup>2</sup>, 0.53 V, and 13.47%, respectively.

Moreover, Figure 7a,b show the secondary ion mass spectrometry (SIMS) data for the PIII 4 KeV and PIII 2 KeV samples. From the SIMS results, we find that the position of nitrogen distribution is shallow and has a high concentration at the a-Si and a-Si/C-Si interface.

**Table 2.** The summary table of without PIII, PIII 2 KeV, PIII 4 KeV, and PIII 6 KeV homojunction solar cells with AlO<sub>x</sub> passivation.

Description	No PIII	PIII 2 KeV	PIII 4 KeV	PIII 6 KeV
$J_{sc}$ (mA/cm <sup>2</sup> )	37.24	37.95	36.95	35.01
$V_{oc}$ (V)	0.46	0.53	0.48	0.52
FF	0.633	0.67	0.595	0.317
$\zeta$ (%)	10.84	13.47	10.546	5.77

**Figure 6.** The I-V characteristic curve of without PIII, PIII 2 Kev, PIII 4 Kev, and PIII 6 Kev homojunction samples.

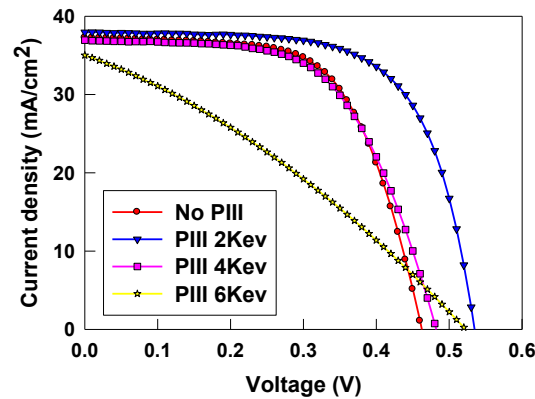
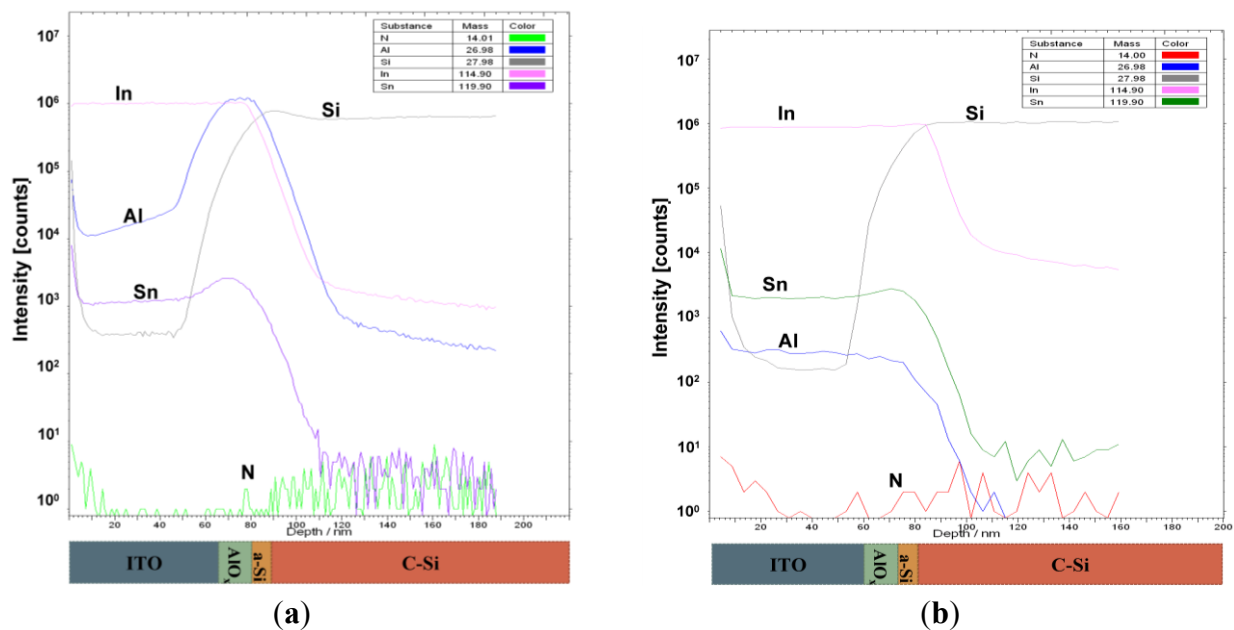


**Figure 7.** (a) The SIMS profiles of PIII 4KeV sample. (b) The SIMS profiles of PIII 2 KeV sample.

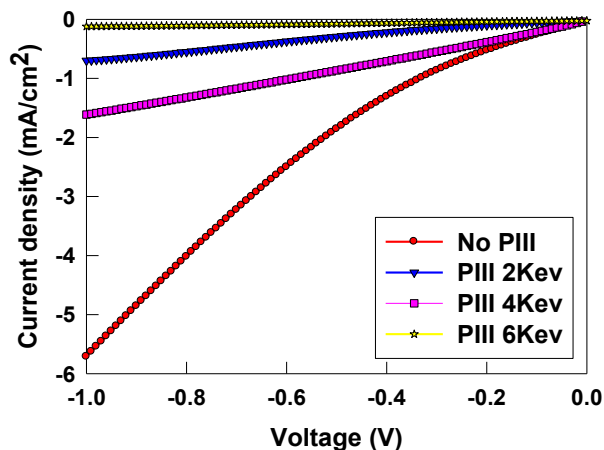


According to the SIMS results, the PIII at 2 keV offered superior depth control than PIII at 4 keV. Therefore, nitrogen can be imported to produce positively charged nitrogen ions, and plasma ions implanted this nitrogen in the device from all sides. Through a lower implantation energy of only 2 keV and higher doses, the number of device defects and dangling bonds in the solar cell can be reduced.

The three conditions were compared based on reverse dark I-V characteristic curves, as shown in Figure 8. From this characteristic, the nitrogen passivation by using PIII can reduce the leakage current. Therefore, PIII passivation of a-Si and c-Si surfaces decreased the defect density and dangling bonds and enhanced the solar cell performance.

Moreover, a homojunction solar cell with  $\text{AlO}_x$  passivation was treated using 2 keV PIII for three periods of time to determine which time period offered superior concentration control: 5 min, 10 min, and 15 min.

**Figure 8.** The reverse dark I-V characteristic curve of solar cell (using heterojunction solar cell with AlO<sub>x</sub> passivation).



Based on the I-V characteristic curves and comparison table shown in Figure 9 and Table 3, the PIII for 10 min offered superior concentration control and passivation. The short-circuit current density ( $J_{sc}$ ), open-circuit voltage ( $V_{oc}$ ), and conversion efficiency were 40.14 mA/cm<sup>2</sup>, 0.54 V, and 13.414%, respectively. Based on the reverse dark I-V characteristic curve shown in Figure 10, the leakage current was also reduced, and the optimized condition was the PIII for 10 min sample.

**Figure 9.** The I-V characteristic curve of without PIII, PIII 2 KeV 5 min, PIII 2 KeV 10 min, and PIII 2 KeV 15 min samples.

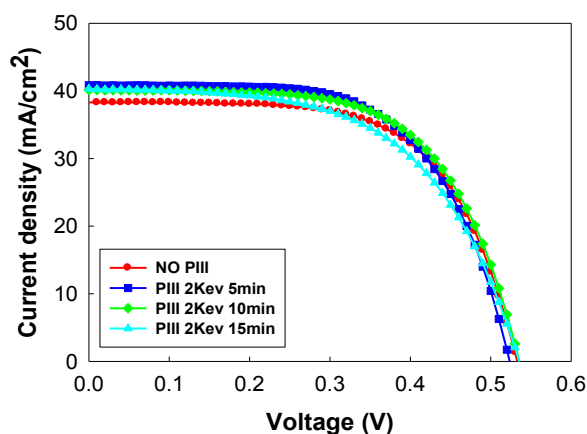
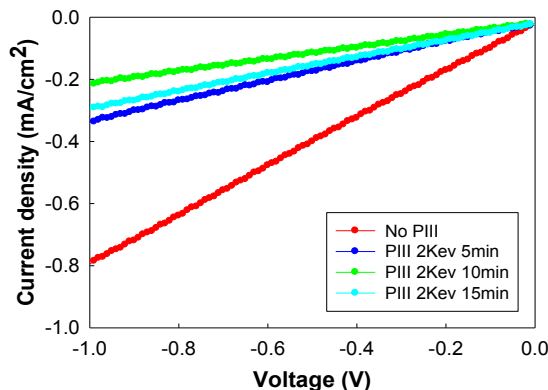


**Table 3.** Summary table of without PIII, PIII 2 KeV 5 min, PIII 2 KeV 10 min, and PIII 2 KeV 15 min homojunction samples without AlO<sub>x</sub> passivation.

Description	No PIII	PIII 5 min	PIII 10 min	PIII 15 min
$J_{sc}$ (mA/cm <sup>2</sup> )	38	40.83	40.14	40.3
$V_{oc}$ (V)	0.53	0.52	0.54	0.54
FF	0.634	0.623	0.619	0.562
$\zeta$ (%)	12.878	13.239	13.414	12.241

**Figure 10.** The reverse dark I-V characteristic curve of solar cell (using homojunction solar cell with AlO<sub>x</sub> passivation).



### 3.3. Optimization of the PIII Condition

Based on these two experiments, PIII at 2 keV for 10 min was demonstrated to yield superior performance. Therefore, this condition was optimized for the passivation of a heterojunction solar cell without AlO<sub>x</sub> passivation. This yielded a superior conversion efficiency of 15.42% from all of the devices, as shown in Figure 11 and Table 4. The short-circuit current density ( $J_{sc}$ ) and open-circuit voltage ( $V_{oc}$ ) were 37.78 mA/cm<sup>2</sup>, and 0.55 V. As Figure 12 shows, the leakage current was also reduced compare with no PIII samples. For these conditions, the number of device defects and dangling bonds can be reduced through PIII in the solar cell.

**Figure 11.** The I-V characteristic curve comparison of without PIII & PIII 2 KeV 10 min heterojunction solar cells without AlO<sub>x</sub>.

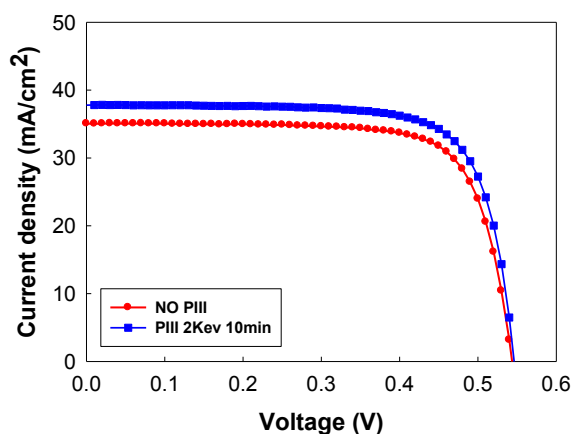
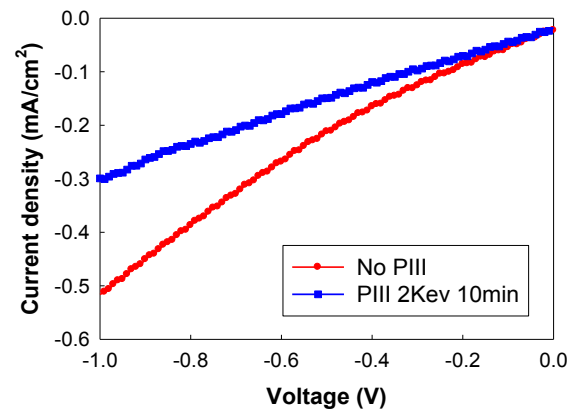


**Table 4.** The summary table of without PIII & PIII 2 KeV 10 min heterojunction solar cells without AlO<sub>x</sub>.

Description	No PIII	PIII 2 KeV
$J_{sc}$ (mA/cm <sup>2</sup> )	35.06	37.78
$V_{oc}$ (V)	0.55	0.55
FF	0.755	0.742
$\eta$ (%)	14.29	15.428

**Figure 12.** The reverse dark I-V characteristic curve of solar cell (using heterojunction solar cell without  $\text{AlO}_x$  passivation).



#### 4. Conclusions

$\text{AlO}_x$  was deposited on a solar cell to passivate the surface by using a fixed charge, to induce the field effect. Solar cell efficiency was enhanced using  $\text{AlO}_x$ , and the  $J_{sc}$  and  $V_{oc}$  values were improved slightly because of the reduction of defects on the c-Si surface by field-effect passivation. PIII was administered at three energy levels; 2 keV offered superior performance, and enhanced the  $J_{sc}$ ,  $V_{oc}$ , and efficiency of the solar cell by effectively reducing the number of dangling bonds on the a-Si and c-Si surfaces. PIII administered for 10 min was found to enhance the  $J_{sc}$ ,  $V_{oc}$ , and efficiency of the solar cell, and effectively reduced the number of dangling bonds on the a-Si and c-Si surfaces. Excess nitrogen atoms were not present in the formation of impurities. The ideal PIII condition (2 keV, 10 min) was used to passivate a heterojunction solar cell without  $\text{AlO}_x$  passivation; the solar cell offered a superior conversion efficiency of 15.42%, a  $J_{sc}$  of 37.78  $\text{mA}/\text{cm}^2$ , a  $V_{oc}$  of 0.55 V, and an FF of 0.742 (AM1.5, area = 1  $\text{cm}^2$ ).

#### Acknowledgments

This project was sponsored by the National Science Council of Taiwan under Contract NSC 102-2221-E-239-034.

#### Author Contributions

In this paper, Yu-Hsien Lin and Yung-Chun Wu contributed to the design and wrote the manuscript. Chun-Hao Chen, Ping-Hua Chen, Yi-He Tsai, and Yi-Yun Yang performed the experiments. All authors collected and analyzed data together. Hsin-Chiang You and K. S. Chang-Liao gave technical support and conceptual advice. All the authors read and approved the manuscript.

#### Conflicts of Interest

The authors declare no conflict of interest.

## References

1. Zhao, J.; Wang, A.; Green, M.A. 24.5% Efficiency silicon PERT cells on MCZ substrates and 24.7% efficiency PERL cells on FZ substrates. *Prog. Photovolt.* **2000**, *7*, 471–474.
2. Okamoto, H.; Hamakawa, Y. A-SiC:H/a-Si:H heterojunction solar cell having more than 7.1% conversion efficiency. *Appl. Phys. Lett.* **1981**, *39*, 237–239.
3. Tsubomura, H.; Matsumura, M.; Nomura, Y.; Amamiya, T. Dye sensitised zinc oxide: Aqueous electrolyte: Platinum photocell. *Nature* **1976**, *261*, 402–403.
4. Liao, K.; Yambem, S.D.; Haldar, A.; Alley, N.J. Seamus. A. Designs and Architectures for the Next Generation of Organic Solar Cells. *Energies* **2010**, *3*, 1212–1250.
5. Hamed, W.A.; Yahya, R.; Bola, A.L.; Mahmud, H.N.M.E. Recent Approaches to Controlling the Nanoscale Morphology of Polymer-Based Bulk-Heterojunction Solar Cells. *Energies* **2013**, *6*, 5847–5868.
6. Ong, P.; Levitsky, I.A. Organic/IV, III-V Semiconductor Hybrid Solar Cells. *Energies* **2010**, *3*, 313–334.
7. Lin, Y.; Wu, Y.; Lai, B. Collection Efficiency Enhancement of Injected Electrons in Dye-sensitized Solar Cells with a Ti Interfacial Layer and TiCl<sub>4</sub> Treatment. *Int. J. Electrochem. Sci.* **2012**, *7*, 9478–9487.
8. Kutsuki, K.; Okamoto, G.; Hosoi, T.; Shimura, T.; Watanabe, H. Germanium oxynitride gate dielectrics formed by plasma nitridation of ultrathin thermal oxides on Ge(100). *Appl. Phys. Lett.* **2009**, *95*, 022102:1–022102:3.
9. Taguchi, M.; Terakawa, A.; Maruyama, E.; Tanaka, M. Obtaining a Higher  $V_{oc}$  in HIT Cells. *Prog. Photovolt. Res. Appl.* **2005**, *13*, 481–488.
10. Wakisaka, K.; Taguchi, M. More than 16% Solar Cells with a New 'HIT' (doped a-Si/nondoped a-Si/crystalline Si). In Proceedings of IEEE, Proceedings of Photovoltaic Specialists Conference, Las Vegas, NV, USA, 7–11 October 1991; Volume 2, pp. 887–892.
11. O'Regan, B.; Gratzel, M. A low-cost, high-efficiency solar cell based on dye-sensitized colloidal TiO<sub>2</sub> films. *Nature* **1991**, *353*, 737–740.
12. Madan, A.; Ovshinsky, S.R.; Czubytyj, W.M. Shur, M. Some Electrical and Optical Properties of a-Si:F:H Alloys. *J. Electron. Mater.* **1980**, *9*, 385–409.
13. Von Maydell, K.; Korte, L.; Laades, A.; Stangl, R.; Conrad, E.; Lange, F.; Schmidt, M. Characterization and Optimization of The Interface Quality in Amorphous/Crystalline Silicon Heterojunction Solar Cells. *J. Non-Cryst. Solids* **2006**, *352*, 1958–1961.
14. Sawada, T.; Terada, N.; Tsuge, S.; Baba, T.; Takahama, T.; Wakisaka, K.; Tsuda, S.; Nakano, S. High-Efficiency a-Si/c-Si Heterojunction Solar Cell. In Proceedings of IEEE Photovoltaic Specialists Conference, Waikoloa, HI, USA, 5–9 December 1994; Volume 2, pp. 1219–1226.
15. Taguchi, M.; Kawamoto, K.; Tsuge, S.; Baba, T.; Sakata, H.; Morizane, M.; Uchihashi, K.; Nakamura, N.; Kiyama, S.; Oota, O. HITTM Cells—High-Efficiency Crystalline Si Cells with Novel Structure. *Prog. Photovolt. Res. Appl.* **2000**, *8*, 503–513.
16. Tsunomura, Y.; Yoshimine, Y.; Taguchi, M.; Baba, T.; Kinoshita, T.; Kanno, H.; Sakata, H.; Maruyama, E.; Tanaka, M. Twenty-Two Percent Efficiency HIT Solar Cell. *Sol. Energy Mater. Sol. Cells* **2009**, *93*, 670–673.

17. Mishima, T.; Taguchi, M.; Sakata, H.; Maruyama, E. Development status of high-efficiency HIT solar cells. *Sol. Energy Mater. Sol. Cells* **2010**, *95*, 18–21.
18. Liu, B. The Applications of Plasma Immersion Ion Implantation to Crystalline Silicon Solar Cells. *Energy Procedia* **2013**, *38*, 289–296.
19. Derbouz, K.; Michel, T.; de Moro, F.; Spiegel, Y.; Torregrosa, F.; Belouet, C.; Slaouil, A. Plasma immersion ion implantation of boron for ribbon silicon solar cells. *EPJ Photovolt.* **2013**, *4*, 45105:1–45105:4.
20. Vervisch, V.; Barakel, D.; Torregrosa, F.; Ottaviani, L.; Pasquinelli, M. Plasma Immersion Ion Implantation Applied to P+N Junction Solar Cells. In Proceedings of the 16th International Conference on Ion Implantation Technology (IIT 2006), Marseille, France, 11–16 November 2006; Volume 886, p. 253.
21. Saint-Cast, P.; Kania, D.; Hofmann, M.; Benick, J.; Rentsch, J.; Preu, R. Very low surface recombination velocity on p-type c-Si by high-rate plasma-deposited aluminum oxide. *Appl. Phys. Lett.* **2009**, *95*, 151502:1–15102:3.
22. Saint-Cast, P.; Benick, J.; Kania, D.; Weiss, L.; Hofmann, M.; Rentsch, J.; Preu, R.; Glunz, S.W. High-Efficiency c-Si Solar Cells Passivated With ALD and PECVD Aluminum Oxide. *IEEE Electron. Device Lett.* **2010**, *31*, 695–697.

© 2014 by the authors; licensee MDPI, Basel, Switzerland. This article is an open access article distributed under the terms and conditions of the Creative Commons Attribution license (<http://creativecommons.org/licenses/by/3.0/>).